THE JOURNAL OF PHYSICAL CHEMISTRY C

Article

pubs.acs.org/JPCC

Stochastic Charge Fluctuations in Bipolar Electrodes

Zinaida A. Kostiuchenko,[†] Bo Zhang,[‡] and Serge G. Lemay*[,†]

[†]MESA+ Institute for Nanotechnology, University of Twente, P.O. Box 217, 7500 AE Enschede, The Netherlands

[‡]Department of Chemistry, University of Washington, Seattle, Washington 98195-1700, United States

ABSTRACT: Bipolar electrodes provide a powerful and versatile means of coupling two or more spatially separated electrochemical reactions. While normally described in terms of macroscopic rate equations, the ongoing drive toward the miniaturization of bipolar electrodes means that new regimes are becoming accessible where stochasticity and the discreteness of the electronic charge become relevant or even dominant. Here we explore using both numerical simulations and analytical theory the behavior of bipolar electrodes with nanoscale dimensions. We focus in particular on the possibility of achieving single-molecule-level synchronization between the two poles of a bipolar electrode, which would dramatically extend the range of applicability of single-molecule electrochemistry. We conclude that, while possible, fundamental limits on the potential dependence of electron-transfer rates dictate that this will only be achieved in the smallest (less than 10 nm) bipolar nanoelectrodes.

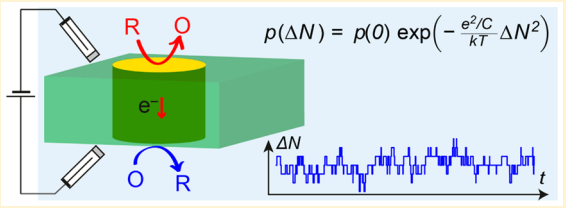

Bipolar electrodes (BPEs) (electrodes that accommodate both oxidation and reduction reactions simultaneously in spatially separated regions of the electrode) are the object of intensive study.[1−3] Application of bipolar electrochemistry principles is remarkably broad and includes material preparation such as creating molecular gradients on a surface,[4] preparing films with nonuniform chemical compositions,[5,6] forming wires,[7] catalytic self-propulsion,[8−11] concentrating analytes inside a capillary[12] or a microchannel,[13−15] sensing based on electrode dissolution,[16] and coupling electrogenerated chemiluminescence[17−21] and fluorescence with other electrochemical reactions.[22,23] The conventional description and understanding of BPE detection principles are however mostly based on macroscopic descriptions in terms of average fluxes and reaction rates, and it has not been fully elucidated to what extent these can be applied to nanoscale experimental systems. This is particularly relevant considering that BPEs may provide a means of studying arbitrary electrochemical reactions at the single-molecule level by coupling a reaction of interest to a reporter reaction that can be detected by fluorescence via a BPE. The experimental realization of this approach, which may prove to be a powerful alternative to single-molecule electrochemical detection based on redox cycling,[24−27] however requires understanding the electrochemical properties of BPEs at the level of individual electron-transfer events.

Here we present a theoretical and numerical analysis of stochastic and single-molecule electrochemistry at meso- and nanoscale BPEs. We show that the number of electrons on such an electrode can undergo large departures from its macroscopically expected value, an effect that can in principle be detected as excess voltage noise at the electrode. We further conclude that as a result of these fluctuations, true single-molecule resolution is only possible in extremely small (order 10 nm or less) electrodes. Interestingly, this behavior bears close analogy to classic single-electron transistors from mesoscopic electronics.[28,29]

THEORY

We concentrate our analysis on a simple, idealized model of an experimentally realizable bipolar system. Since the main conclusions of our analysis turn out to be largely independent of the details of the model, this allows concentrating on the key concepts without being encumbered by unnecessarily complex notation. We comment on more complex experimental situations in the Results and Discussion section.

Consider a single BPE imbedded in an insulating membrane such that it contacts two reservoirs, as sketched in Figure 1. The electrode is cylindrical with radius r and length l. The first reservoir contains a single species that can be oxidized, $R_{(1)} \rightarrow O_{(1)} + e^-$, while the second contains a single species that can be reduced, $O_{(2)} + e^- \rightarrow R_{(2)}$. The two reservoirs are under potential control via reference electrodes, and a potential difference V can be applied between them. For more complex geometries, e.g., where the driving electrodes are located far from the BPE and significant ohmic drops occur between the reference and the BPE, the potentials employed in the model correspond to the local potentials at the electrolyte/BPE interfaces. Under steady-state conditions, the oxidation and reduction rates at the BPE in the two reservoirs (k_O and k_R, respectively, expressed as an average number of electron transfer events per unit time) balance out and a constant average electrical current flows from reservoir 2 to reservoir 1 via the BPE. Equating of the two rates is rendered possible by the potential of the bipolar electrode, which is free to self-adjust until the steady-state condition is satisfied.

Received: May 11, 2016
Revised: September 12, 2016
Published: September 16, 2016

DOI: 10.1021/acs.jpcc.6b04767
J. Phys. Chem. C 2016, 120, 22777−22783

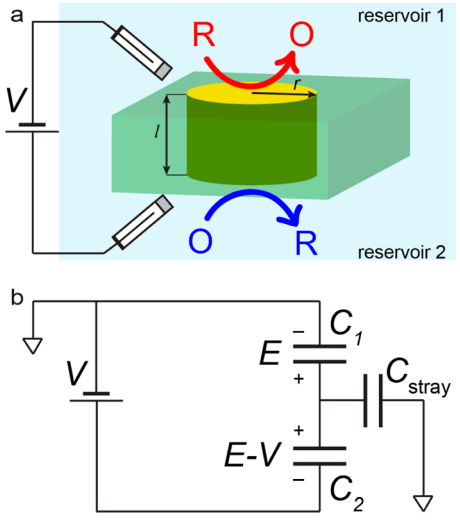

Figure 1. (a) Sketch of the experimental configuration showing the BPE (yellow) and the two reservoirs. (b) Corresponding equivalent circuit when no electron transfer is taking place.

The oxidation rate in reservoir 1 is a function of the bipolar electrode potential with respect to the reference electrode in reservoir 1, a potential difference that we call E. For the specific case of a reversible, diffusion-limited oxidation reaction in the presence of a supporting electrolyte in reservoir 1, the rate of oxidation takes the simple form

$$k_O(E) = \frac{k_{O,lim}}{\exp\left(\frac{-e(E-E_O)}{kT}\right) + 1} \tag{1a}$$

Here E_O is the formal potential of the reaction, k is the Boltzmann constant, and T is the absolute temperature. For a shrouded disk electrode contacting reservoir 1, the constant $k_{O,lim}$ has the value $k_{O,lim} = 4Drc$, where D is the diffusion coefficient of the reduced species in reservoir 1, r is the radius of the electrode as defined in Figure 1, and c is the number density of reduced molecules in reservoir 1. Equation 1a assumes a nonzero steady-state current, as is readily achieved at micro- and nanoscale electrodes.

Simultaneously, the reduction reaction can take place at the other end of the bipolar electrode. Under the same assumptions as above, the reduction rate has the form

$$k_R(E) = \frac{k_{R,lim}}{\exp\left(\frac{+e(E-V-E_R)}{kT}\right) + 1} \tag{1b}$$

where E_R is the formal potential of the reduction reaction. Note that V appears in eq 1b because it is the potential difference between the bipolar electrode and reservoir 2, $E - V$, that drives this reaction. Since an applied potential V is equivalent to a shift in E_R as per eq 1b, however, we choose $V = 0$ throughout and represent all changes to reservoir 2 as shifts in E_R without loss of generality.

In a steady-state situation, the net current into or out of the bipolar electrode must be zero. In other words, in the steady-state, the bipolar electrode potential must drift to a value E_{ss} such that $k_O(E_{ss}) = k_R(E_{ss})$. Solving for E_{ss} using eqs 1a and 1b then yields

$$E_{ss} = \frac{kT}{e}\ln\left\{\frac{\frac{k_{R,lim}}{k_{O,lim}} - 1}{2}\exp\left(\frac{e}{kT}E_R\right) + \frac{1}{2}\sqrt{\left(1 - \frac{k_{R,lim}}{k_{O,lim}}\right)^2\exp\left(\frac{2e}{kT}E_R\right) + 4\frac{k_{R,lim}}{k_{O,lim}}\exp\left(\frac{e}{kT}(E_O + E_R)\right)}\right\} \tag{2}$$

The shift in potential E reflects the accumulation of a net charge on the electrode. Each time that an electron is added to $(N \rightarrow N + 1, \Delta N = +1)$ or removed from $(N \rightarrow N - 1, \Delta N = -1)$ the electrode, elementary circuit theory indicates that the electrode potential shifts by a value

$$\Delta E = \frac{-e}{C_1 + C_2 + C_{stray}}\Delta N = \frac{-e}{C_{tot}}\Delta N \tag{3}$$

Here $-e$ is the charge of the electron, C_1 and C_2 are the double-layer capacitances of the ends of the bipolar electrode in contact with reservoir 1 and reservoir 2, respectively, and C_{stray} is the stray capacitance due the electric field penetrating the insulating material surrounding the bipolar electrode. For simplicity we assume that all of these capacitances are independent of potential. To simplify the notation, we also defined the total bipolar electrode capacitance, $C_{tot} = C_1 + C_2 + C_{stray}$.

Estimates of the value of C_{tot} for BPEs with different dimensions are given in Table 1. For the double-layer capacitances C_1 and C_2 we use a typical experimental value of 20 μF/cm^2 for the Pt(111) surface[30] and a surface area of πr^2, where r is the radius of the electrode. To estimate the stray capacitance, we model the BPE as a cylinder oriented perpendicular to a conducting plane which represents the electrolyte. Assuming that the length of the electrode is much larger than its diameter, this yields[31]

$$C_{stray} \approx \frac{2\pi\varepsilon_r\varepsilon_0 l}{\ln\left(\frac{l}{r\sqrt{3}}\right)} \tag{4}$$

where l is the height of BPE, r is its radius, ε_r is the relative permittivity of the insulating membrane material (here we use a value of 3.9 corresponding to silicon dioxide), and ε_0 is the

Table 1. Stray Capacitance and Double Layer Capacitance for BPEs of Different Sizes

radius r (nm)	length l (nm)	C_{stray} (F)	C_1, C_2 (F)	C_{tot} (F)	e/C_{tot} (V)
1	10	1.2×10^{-18}	6.3×10^{-19}	2.5×10^{-18}	6.4×10^{-2}
10	100	1.2×10^{-17}	6.3×10^{-17}	1.4×10^{-17}	1.2×10^{-3}
50	500	6.2×10^{-17}	1.6×10^{-15}	3.2×10^{-15}	5.0×10^{-5}
100	1000	1.2×10^{-16}	6.3×10^{-15}	1.3×10^{-14}	1.3×10^{-5}
200	2000	2.5×10^{-16}	2.5×10^{-14}	5.1×10^{-14}	3.2×10^{-6}
500	5000	6.2×10^{-16}	1.6×10^{-13}	3.1×10^{-13}	5.1×10^{-7}
1000	10000	1.2×10^{-15}	6.3×10^{-13}	1.3×10^{-12}	1.3×10^{-7}

DOI: 10.1021/acs.jpcc.6b04767
J. Phys. Chem. C 2016, 120, 22777−22783

vacuum permittivity. Strictly speaking, this expression represents a lower bound for C_{stray} because our experimental configuration includes two reservoirs located at both ends of the BPE rather than a single reservoir, but this discrepancy causes only a correction of order unity in the argument of the logarithm and is not quantitatively significant.

Equation 3 carries an important qualitative message: because the shift in electrode potential is proportional to e/C_{tot}, the impact of adding or subtracting a single electron from the BPE becomes more pronounced with decreasing capacitance and hence with decreasing electrode size. For example, Table 1 indicates that micrometer-scale BPEs have capacitances on the order of 1 pF, leading to ΔE of order 100 nV. Since the oxidation and reduction rates given by eq 1a and eq 1b only vary significantly when E changes by an amount of order kT/e, or 25 mV at room temperature, for such large electrodes the addition or extraction of a single electron cannot be expected to have a large impact on the rates of the following oxidation or reduction event. Furthermore, since ΔE is proportional to C_{tot}, it is necessary for all three contributions to the capacitance (C_1, C_2, and C_{stray}) to be small for ΔE to become large. If the two electrodes are of different sizes, for example, the larger of the two electrodes will dominate the quantization behavior and determine to what extent single electron transfer events influence electron transfer.

Mesoscopic Description. In order to account for single electron-transfer events, it becomes necessary to follow the electrode potential $E(t)$ as a function of time t. Such an explicit description of electron transport has been explored in detail in the context of solid-state quantum dots,[28,29] where it is known as full counting statistics.[32,33]

Explicitly following $E(t)$ is equivalent to keeping track of the charge on the BPE, as indicated by eq 3. For this purpose we introduce the variable $\Delta N(t)$, which represents the departure of the number of electrons on the bipolar electrode from its macroscopically expected steady-state value when $E = E_{ss}$. That is, $\Delta N = 0$ corresponds to the steady-state potential E_{ss} for which $k_O(E) = k_R(E)$. Any other value of ΔN corresponds to a shift in BPE potential as per eq 3.

When $\Delta N \neq 0$, k_O is no longer equal to k_R. Inspection of eqs 1−3 shows that the shift in potential resulting from $\Delta N \neq 0$ favors either k_O or k_R in such a way that ΔN tends to return toward 0. This is illustrated in Figure 2, where it is seen explicitly that adding an electron ($\Delta N = +1$) favors a subsequent reduction reaction ($k_R > k_O$) while extracting an electron ($\Delta N = -1$) favors subsequent oxidation. Electron transfer is a stochastic process, however: while on average the system will return toward $\Delta N = 0$, there is a finite chance that, for example, a reduction event is followed by a second reduction instead of a compensating oxidation.

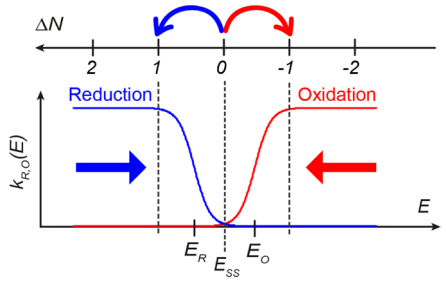

Figure 2. Top: Axis representing the number of electrons on the BPE. $\Delta N = 0$ corresponds to the number of electrons present when the electrode potential is equal to its average macroscopic value, E_{ss}. Bottom: Oxidation and reduction rates in the two reservoirs as a function of electrode potential, E, and corresponding electron number, ΔN. Here the potential difference for adding or removing an electron is sufficient to modify the oxidation and reduction rates significantly, which corresponds to very small values of C_{tot}, the capacitance of the BPE.

This description assumes that after each reduction or oxidation event the electrode potential has time to equilibrate before the next event. This implicitly supposes that the time interval between two electron-transfer events, δt, is longer than the time τ required for the BPE to come to a new equilibrium with the reservoir, or $\tau/\delta t \ll 1$. The time τ is simply the time constant of the RC circuit defined by the double-layer capacitance and the access resistance of the BPE. For two shrouded disk electrodes in parallel, this is given by $R = {}^1/_{8sr}$, where s is the conductivity of the electrolyte and r is radius of the BPE.[34] The time δt can be estimated as redox current related to an elementary charge. Hence,

$$\frac{\tau}{\delta t} = \frac{C}{8sr}\frac{I}{e}$$

Supposing a 0.1 M KCl aqueous solution with a conductivity[35] of 1.48 S/m yields τ of ∼0.1 μs and 0.2 ns for the largest and the smallest electrodes in Table 1, respectively, indicating that the relaxation condition is satisfied for currents smaller than 1 pA (6×10^6 electrons/s) and 1 nA (6×10^9 electrons/s), respectively.

What is the probability of ΔN deviating significantly from zero? And what is the typical size of the fluctuations in ΔN that one can expect? Answering these questions is the aim of the following analysis.

Simulations. To better visualize the process of electron transfer from one reservoir to another via the BPE, we first present numerical simulations of eqs 1−3 that illustrate the real-time evolution of ΔN and the accompanying sequence of oxidation and reduction events. The simulations assume that the BPE starts in its equilibrium configuration, $\Delta N = 0$. In each time interval Δt thereafter, there is a probability $k_O(\Delta N)\Delta t$ that an oxidation event takes place in reservoir 1, in which case $\Delta N \rightarrow \Delta N + 1$. There is also a corresponding probability $k_R(\Delta N)\Delta t$ that a reduction event takes place in reservoir 2 ($\Delta N \rightarrow \Delta N - 1$). The selected value of Δt was sufficiently small that the probability of more than one electron-transfer event taking place during one simulation step was negligible ($k_O(\Delta N)\Delta t$ and $k_R(\Delta N)\Delta t$ were ≤0.01). Once an oxidation or reduction event occurred, the number of electrons inside the BPE, ΔN, was increased or decreased by 1 and its potential correspondingly adjusted by $-e\Delta N/C_{tot}$. These new values were used immediately in the next time step; this is valid so long as the electron-transfer rates are much smaller than the relaxation time of the BPE, as discussed above. The simulation was implemented in Matlab 8.4.0 using the binornd() function for random number generation.

There are effectively four experimental parameters characterizing the system, namely, $k_{O,lim}$, $k_{R,lim}$, $E_O - E_R$, and C_{tot}. The first three depend on the faradaic processes taking place in solution while the last reflects the properties of the BPE itself. For the illustrative simulations below we take $k_{O,lim} = k_{R,lim} = 1$ s^{-1}, $E_O - E_R = 0.2$ V, corresponding to Figure 2.

A typical trace of $\Delta N(t)$ for $C_{tot} = 10^{-17}$ F is shown in Figure 3a and Figure 3b (zoom-in). Over the course of the simulated interval, the system performs discrete jumps between six

DOI: 10.1021/acs.jpcc.6b04767
J. Phys. Chem. C 2016, 120, 22777−22783

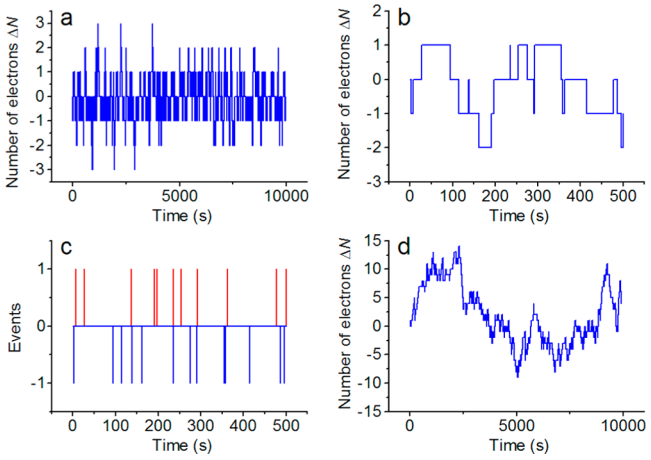

Figure 3. (a) Time trace of the number of electrons ΔN for a BPE with capacitance $C_{tot} = 10^{-17}$ F. (b) Zoomed-in part of panel a showing additional detail. (c) Time trace illustrating the sequence of reduction (blue spikes) and oxidation (red spikes) events corresponding to trace b. (d) Time trace of ΔN for a BPE with a capacitance of 10^{-12} F.

discrete states, each upward jump ($\Delta N \rightarrow N + 1$) corresponding to oxidation of one molecule in reservoir 1 and each downward jump ($\Delta N \rightarrow \Delta N - 1$) to a reduction event in reservoir 2. This is more explicitly illustrated in Figure 3c, where positive and negative spikes represent the timing of individual oxidation and reduction events. It is clear that reduction and oxidation events do not necessarily alternate and that successive events of the same type are common. The latter becomes even more true for electrodes with a larger capacitance, as illustrated in Figure 3d ($C_{tot} = 10^{-12}$ F, other parameters unchanged). Over the course of this typical time trace, 424 individual electron transfer events take place and ΔN is seen to span a range of 23 different values.

In order to summarize the stationary, steady-state properties of time traces such as those shown in Figure 3, we performed longer simulations and computed histograms of the probability of the system to be found in states characterized by different values of ΔN (the simulations were run for a sufficiently long time that the histograms became independent of the simulation time). Figure 4 shows the occupation probability as a function

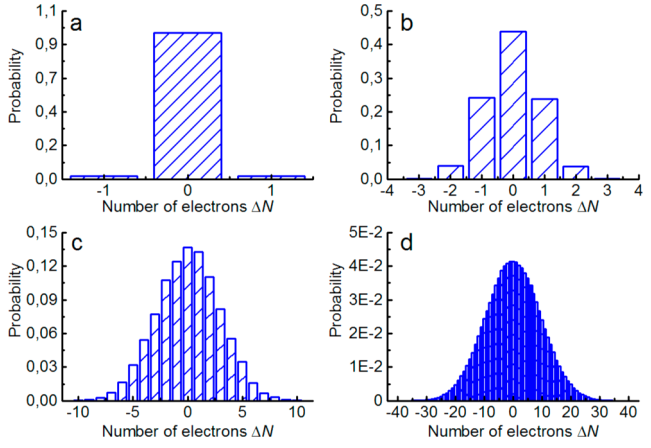

Figure 4. Simulated probability distributions for values of the capacitance C_{tot} of (a) 10^{-18} F, (b) 10^{-17} F, (c) 10^{-16} F, and (d) 10^{-15} F. Other parameters were $E_O - E_R = 0.2$ V, $k_R = k_O = 1$ s^{-1}.

of ΔN for several values of the capacitance C_{tot}, the other parameters being identical to those of Figure 3. For an ultralow capacitance of 10^{-18} F (Figure 4a), corresponding to an electrode only a few nanometers in size as per Table 1, the system spends most of its time in the $\Delta N = 0$ state, with only rare excursions to other states. Here the microscopic state of the BPE can be said to be well-defined. For a capacitance of 10^{-17} F (Figure 4b), the histogram instead reflects the time traces of Figure 3a and Figure 3b, with a handful of states being visited with significant probability. Figure 4c and Figure 4d show that the same trend continues with further increases in capacitances: the absolute size of the excursions in ΔN increases with increasing C_{tot}.

Analytical Solution. While the simulations presented above explicitly illustrate the nature of the electron number fluctuations present in BPEs, it is useful, especially for guiding to experiments, to generalize these results to broadly applicable analytical expressions. With this in mind, we introduce the probability $p_{\Delta N}$ that the BPE is found at a given instant $t_0 + \Delta t$ in a state with exactly ΔN electrons. There are three ways for the BPE to arrive into such a state depending on its state at the previous instant t_0, as summarized in Figure 5: start in a state

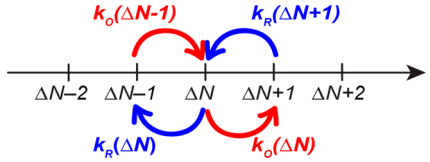

Figure 5. Scheme of reduction (blue) and oxidation (red) processes around the state ΔN.

with exactly ΔN electrons and remain unchanged, start in a state with $\Delta N - 1$ electrons and gain an electron via an oxidation reaction in reservoir 1, or start in a state with $\Delta N + 1$ electrons and lose an electron via reduction in reservoir 2. The corresponding time evolution is given by

$$\frac{\partial p_{\Delta N}}{\partial t} = p_{\Delta N-1} k_O(\Delta N - 1) + p_{\Delta N+1} k_R(\Delta N + 1) - p_{\Delta N}[k_O(\Delta N) + k_R(\Delta N)] \quad (5)$$

A stationary steady state is achieved when $\partial p\Delta N/\partial t = 0$; moreover, since $p_{\Delta N} \rightarrow 0$ for $\Delta N \rightarrow \pm\infty$, the steady state solution must necessarily satisfy detailed balance,

$$p_{\Delta N-1} k_O(\Delta N - 1) = p_{\Delta N} k_R(\Delta N) \quad (6)$$

Recursively applying this relation over subsequent values of ΔN yields the full distribution for $p_{\Delta N}$,

$$\frac{p_{\Delta N}}{p_0} = \prod_{k=0}^{\Delta N-1} \frac{k_O(k)}{k_R(k+1)} \quad (7a)$$

$$\frac{p_{-\Delta N}}{p_0} = \prod_{k=0}^{\Delta N-1} \frac{k_R(-k)}{k_O(-k-1)} \quad (7b)$$

where p_0 is the probability that the number of electrons is $\Delta N = 0$. This expression is general and complete except for the overall normalization factor p_0 which can be determined by requiring that the sum of the values of $p_{\Delta N}$ for all ΔN is unity.

As a simple application of eq 7, consider the case where the steady-state BPE potential E_{ss} lies in the decaying tails of both

DOI: 10.1021/acs.jpcc.6b04767
J. Phys. Chem. C 2016, 120, 22777−22783

the oxidation and the reduction reaction, as per Figure 2 (that is, $E_O - E_{ss} \gg kT/e$, $E_{ss} - E_R \gg kT/e$) . The rate equations (eqs 1a and 1b) are then approximately exponential,

$$k_O(\Delta E) \approx k_{O,lim} \exp\left(\frac{-e(E_O - E_{ss} - \Delta E)}{kT}\right)$$

$$k_R(\Delta E) \approx k_{R,lim} \exp\left(\frac{-e(E_{ss} - E_R + \Delta E)}{kT}\right)$$

In this case eq 7 can be computed explicitly to yield

$$\frac{p_{\Delta N}}{p_0} = \left(\frac{k_{O,lim}}{k_{R,lim}}\right)^{\Delta N} \exp\left\{\frac{e\Delta N}{kT}[2E_{ss} - (E_O + E_R)]\right\} \exp\left\{-\frac{\frac{e^2}{C_{tot}}}{kT}\Delta N^2\right\} \quad (8)$$

Furthermore, since in this limit the steady-state potential is given by $E_{ss} = (E_R + E_O)/2 + \left(\frac{kT}{2e}\right)\ln(k_R/k_O)$, eq 8 reduces to the simple form

$$\frac{p_{\Delta N}}{p_0} = \exp\left\{-\frac{e^2/C_{tot}}{kT}\Delta N^2\right\} \quad (9)$$

Evaluating p_0 from the normalization condition and denoting $\sigma = \sqrt{\frac{kT}{2e^2/C_{tot}}}$ yields our final result,

$$p_{\Delta N} = \frac{1}{\sigma\sqrt{2\pi}} \exp\left(-\frac{\Delta N^2}{2\sigma^2}\right) \quad (10)$$

This expression takes the form of a Gaussian around the steady-state average, $\Delta N = 0$, with a standard deviation given by $\sqrt{\frac{kT}{2e^2/C_{tot}}}$. This result is in quantitative agreement with the simulations down to capacitance values of 10^{-18} F, as shown in Figure 6 (a slight discrepancy arises for 10^{-18} F because $p_{\Delta N}$ was normalized assuming a continuous distribution, whereas in this case the simulated curve exhibits heavy discretization).

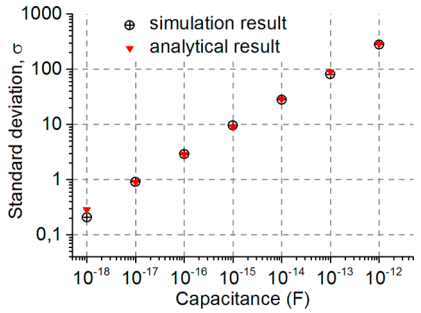

Figure 6. Standard deviation of the probability distributions obtained from simulations and analytical results ($E_O - E_R = 0.2$ V, $k_{R,lim} = k_{O,lim} = 1$ s^{-1}).

Interestingly, eq 9 is reminiscent of an equilibrium Boltzmann distribution for the electrostatic energy stored in C_{tot}. We emphasize that the expression is not an equilibrium result, however, as is made explicit by the fact that, in general, the distribution $p_{\Delta N}$ depends on the kinetic parameters $k_{O,lim}$ and $k_{R,lim}$.

RESULTS AND DISCUSSSION

Stochastic fluctuations. Our results indicate that the fluctuations in the number of electrons, ΔN, are much larger than unity for all but the smallest nanoelectrodes and become larger with increasing electrode size. This may appear counterintuitive given that fluctuations in ΔN are largely irrelevant in experiments with macroscopic or micrometer-scale BPEs. Note however that the number of electrons residing on the BPE is not directly observable experimentally. More relevant is the size of the fluctuations of the electrode potential, E, which can be derived by combining eqs 3 and 10 to yield

$$\delta E_{rms} = \sqrt{\frac{kT}{2C_{tot}}} \quad (11)$$

This expression indicates that the size of the voltage fluctuations decreases with increasing electrode size (since C_{tot} increases with electrode size) and vanishes in the limit of macroscopic electrodes, consistent with intuition. For a nanoelectrode with $C_{tot} = 10^{-17}$ F, eq 11 predicts very sizable voltage fluctuations of 14 mV_{rms}. In order to measure these fluctuations with, for example, an external electrometer, however, it would be necessary to provide an electrical connection to the BPE. The typical capacitance of such a wire is typically >1 pF, dwarfing the intrinsic capacitance of the BPE and limiting the magnitude of the fluctuations to 45 μV_{rms} or less. While still observable with a dedicated experiment, such fluctuations would be too small to have a readily observable influence on the properties of the BPE.

Single-Molecule Measurements. A particularly intriguing possibility is with nanoscale BPEs to perform one-to-one mapping between single-molecule oxidation and reduction events in the two reservoirs. This is possible only in the case of a narrow probability distribution with only a few discrete states separated in potential by more than kT/e being occupied. Our results indicate that this occurs when $\sigma = \sqrt{\frac{kT}{2e^2/C_{tot}}} < 1$, which as seen above corresponds to capacitances of order 10^{-18} F or less at room temperature. On the basis of the estimates of Table 1, this is possible to realize experimentally but requires electrodes only a few nanometers in size. Such small dimensions would be highly challenging to realize using top–down lithographic approaches but may be achievable by, for example, imbedding nanoparticles in an insulating membrane.

Even with such extremely small electrodes, however, the discrete electron transport includes an additional random factor that is difficult to control experimentally. In both the simulations and analytical calculations presented above, we have assumed that the discrete state $\Delta N = 0$ corresponds exactly to the macroscopic steady-state potential, E_{ss}. In general there is no reason why this ought to be the case, however: the value of E_{ss} obtained from the macroscopic rate equations may also correspond to a potential that falls between two of the allowed discrete states. This is illustrated in Figure 7, which shows the probability distribution $p_{\Delta N}$ for four different values of E_{ss} with respect to the discrete electronic states. If E_{ss} falls precisely in the middle of the gap between two states (Figure 7a), finding the system in either of these two states is equally probable. In this case the BPE oscillates between the two states (0 and +1 in the figure), and alternating oxidation and reduction reactions take place in the two reservoirs. If instead E_{ss} corresponds exactly to one of the discrete states (Figures 4a and 7d), the system spends most of its time in the state with E

DOI: 10.1021/acs.jpcc.6b04767
J. Phys. Chem. C 2016, 120, 22777−22783

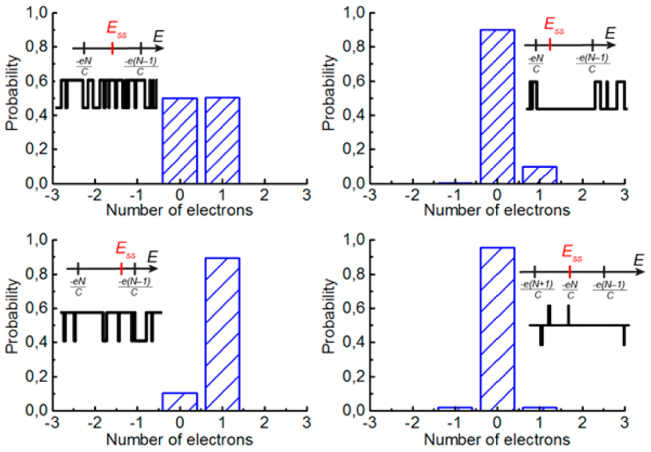

Figure 7. Simulated probability distributions for the cases where the equilibrium potential E_{ss} lies halfway between two discrete electronic states (a, upper left), at 0.25 of the energy difference between two states (b, upper right), at 0.75 of the difference (c, lower left), and in perfect coincidence with one of the discrete state (d, lower right). $E_O - E_R = 0.2$ V, $C_{tot} = 10^{-18}$ F, $k_{R,lim} = k_{O,lim} = 1$ s^{-1}.

$= E_{ss}$. Either an oxidation reaction in reservoir 1 or a reduction reaction in reservoir 2 can then take place with equal probability; in each case the corresponding reduction/oxidation then takes place quickly in the other reservoir, bringing the system back to the starting $\Delta N = 0$ state. Other cases (Figure 7b and Figure 7c) break the symmetry, with either a reduction or an oxidation being favored as initial step in the cycle. Importantly, there would be no way to control a priori which of the cases in Figure 7 would be realized in an experiment: even nominally identical electrodes could exhibit different potential offsets due to minor differences in capacitance or static charges in the environment, making it difficult to distinguish between the various scenarios and thus complicating interpretation.

Generality of Results. Both the simulations and the analytical results presented above were derived for the specific case of reversible electron-transfer kinetics, as defined by eqs 1a and 1b. Could nonideal kinetics result in smaller fluctuations, thus also facilitating single-molecule measurements? A general answer is provided by eq 7, which indicates that the sharpness of the peak in $p_{\Delta N}$ is dictated by how abruptly the electron-transfer rates vary with varying ΔN or, equivalently, with the electrode potential E. Reversible kinetics represent the sharpest achievable gradient in the rate functions $k_{O,R}(E)$, being in this case only limited by the (Fermi–Dirac) distribution of electron energies in the electrode. Quasi-reversible or irreversible reactions instead exhibit a weaker dependence of k_O and k_R on E, which translates into a more slowly varying distribution $p_{\Delta N}$ and correspondingly larger fluctuations in ΔN. The fluctuations are also larger for systems where the conditions $E_O - E_{ss} \gg kT/e$ or $E_{ss} - E_R \gg kT/e$ are not satisfied, since then $k_O(E)$ and/or $k_R(E)$ approaches a constant value and the dependence of $p_{\Delta N}$ on ΔN becomes weaker. Equation 10 thus corresponds to a lower bound for the size of the fluctuations in ΔN, and less ideal kinetics will result in larger fluctuations.

Another possible limitation to the applicability of our results is that they are derived for the case of a stationary steady state. In some experiments it may be possible to initially prepare the BPE away from this condition ($E \neq E_{ss}$). However, preparing the BPE at, for example, a highly oxidizing potential would mean that there would be a high likelihood that multiple oxidizing events would take place in succession. In this case one pole of the BPE is temporarily functioning as a conventional electrode, with no compensating reaction taking place at the other pole. Coupling between the two reservoirs is only re-established once E approaches E_{ss}, at which point the results derived here start to hold.

CONCLUSIONS

We have considered theoretically the microscopic stochastic fluctuations taking place when a BPE is employed to couple electrochemical reactions at its two poles. We showed that the number of electrons residing on the BPE (and, correspondingly, the electrode potential) fluctuates as a result of the random faradaic processes. The potential fluctuations become vanishingly small for macroscopic electrodes, making a conventional description in terms of average fluxes appropriate. The potential excursions can however become sufficiently large at ultrasmall electrodes that a one-to-one coupling between single-molecule oxidation and reduction events at the two poles of the BPE can in principle be established. The latter requires BPEs of a few nanometers in size. Indeed, the condition for achieving single-molecule coupling, $e^2/C_{tot} > kT$, is equivalent to the condition for observing the Coulomb blockade effect in metal nanoparticles.[36−42] The experimental realization of a BPE on this scale thus represents a very significant technical challenge but would open the door to a new generation of single-molecule electrochemistry measurements far beyond the present state of the art.

AUTHOR INFORMATION

Corresponding Author

*E-mail: s.g.lemay@utwente.nl.

Author Contributions

The manuscript was written through contributions of all authors. All authors have given approval to the final version of the manuscript.

Notes

The authors declare no competing financial interest.

ACKNOWLEDGMENTS

The authors gratefully acknowledge fruitful discussions with Y. M. Blanter. This work was financially supported by the European Research Council (ERC) under Project 278801.

REFERENCES

(1) Loget, G.; Kuhn, A. Shaping and exploring the micro- and nanoworld using bipolar electrochemistry. *Anal. Bioanal. Chem.* **2011**, *400*, 1691−1704.

(2) Loget, G.; Zigah, D.; Bouffier, L.; Sojic, N.; Kuhn, A. Bipolar Electrochemistry: From Materials Science to Motion and Beyond. *Acc. Chem. Res.* **2013**, *46*, 2513−2523.

(3) Fosdick, S. E.; Knust, K. N.; Scida, K.; Crooks, R. M. Bipolar Electrochemistry. *Angew. Chem., Int. Ed.* **2013**, *52*, 10438−10456.

(4) Ulrich, C.; Andersson, O.; Nyholm, L.; Björefors, F. Formation of Molecular Gradients on Bipolar Electrodes. *Angew. Chem., Int. Ed.* **2008**, *47*, 3034−3036.

(5) Ramakrishnan, S.; Shannon, C. Display of Solid-State Materials Using Bipolar Electrochemistry. *Langmuir* **2010**, *26*, 4602−4606.

(6) Inagi, S.; Ishiguro, Y.; Atobe, M.; Fuchigami, T. Bipolar Patterning of Conducting Polymers by Electrochemical Doping and Reaction. *Angew. Chem., Int. Ed.* **2010**, *49*, 10136−10139.

(7) Bradley, J.-C.; Chen, H.-M.; Crawford, J.; Eckert, J.; Ernazarova, K.; Kurzeja, T.; Lin, M.; McGee, M.; Nadler, W.; Stephens, S. G.

DOI: 10.1021/acs.jpcc.6b04767
J. Phys. Chem. C 2016, 120, 22777−22783

Creating electrical contacts between metal particles using directed electrochemical growth. *Nature* **1997**, *389*, 268−271.
(8) Wang, Y.; Hernandez, R. M.; Bartlett, D. J.; Bingham, J. M.; Kline, T. R.; Sen, A.; Mallouk, T. E. Bipolar Electrochemical Mechanism for the Propulsion of Catalytic Nanomotors in Hydrogen Peroxide Solutions. *Langmuir* **2006**, *22*, 10451−10456.
(9) Mano, N.; Heller, A. Bioelectrochemical Propulsion. *J. Am. Chem. Soc.* **2005**, *127*, 11574−11575.
(10) Loget, G.; Kuhn, A. Electric field-induced chemical locomotion of conducting objects. *Nat. Commun.* **2011**, *2*, 535.
(11) Sentic, M.; Loget, G.; Manojlovic, D.; Kuhn, A.; Sojic, N. Light-Emitting Electrochemical "Swimmers". *Angew. Chem., Int. Ed.* **2012**, *51*, 11284−11288.
(12) Wei, W.; Xue, G.; Yeung, E. S. One-Step Concentration of Analytes Based on Dynamic Change in pH in Capillary Zone Electrophoresis. *Anal. Chem.* **2002**, *74*, 934−940.
(13) Dhopeshwarkar, R.; Hlushkou, D.; Nguyen, M.; Tallarek, U.; Crooks, R. M. Electrokinetics in Microfluidic Channels Containing a Floating Electrode. *J. Am. Chem. Soc.* **2008**, *130*, 10480−10481.
(14) Anand, R. K.; Johnson, E. S.; Chiu, D. T. Negative Dielectrophoretic Capture and Repulsion of Single Cells at a Bipolar Electrode: The Impact of Faradaic Ion Enrichment and Depletion. *J. Am. Chem. Soc.* **2015**, *137*, 776−783.
(15) Knust, K. N.; Hlushkou, D.; Anand, R. K.; Tallarek, U.; Crooks, R. M. Electrochemically Mediated Seawater Desalination. *Angew. Chem., Int. Ed.* **2013**, *52*, 8107−8110.
(16) Chow, K.-F.; Chang, B.-Y.; Zaccheo, B. A.; Mavré, F.; Crooks, R. M. A Sensing Platform Based on Electrodissolution of a Ag Bipolar Electrode. *J. Am. Chem. Soc.* **2010**, *132*, 9228−9229.
(17) Arora, A.; Eijkel, J. C. T.; Morf, W. E.; Manz, A. A Wireless Electrochemiluminescence Detector Applied to Direct and Indirect Detection for Electrophoresis on a Microfabricated Glass Device. *Anal. Chem.* **2001**, *73*, 3282−3288.
(18) Wu, M.-S.; Qian, G.-s.; Xu, J.-J.; Chen, H.-Y. Sensitive Electrochemiluminescence Detection of c-Myc mRNA in Breast Cancer Cells on a Wireless Bipolar Electrode. *Anal. Chem.* **2012**, *84*, 5407−5414.
(19) Zhan, W.; Alvarez, J.; Crooks, R. M. Electrochemical Sensing in Microfluidic Systems Using Electrogenerated Chemiluminescence as a Photonic Reporter of Redox Reactions. *J. Am. Chem. Soc.* **2002**, *124*, 13265−13270.
(20) Zhai, Q.; Zhang, X.; Han, Y.; Zhai, J.; Li, J.; Wang, E. A Nanoscale Multichannel Closed Bipolar Electrode Array for Electrochemiluminescence Sensing Platform. *Anal. Chem.* **2016**, *88*, 945−951.
(21) Wu, S.; Zhou, Z.; Xu, L.; Su, B.; Fang, Q. Integrating bipolar electrochemistry and electrochemiluminescence imaging with microdroplets for chemical analysis. *Biosens. Bioelectron.* **2014**, *53*, 148−153.
(22) Oja, S. M.; Guerrette, J. P.; David, M. R.; Zhang, B. Fluorescence-Enabled Electrochemical Microscopy with Dihydroresorufin as a Fluorogenic Indicator. *Anal. Chem.* **2014**, *86*, 6040−6048.
(23) Ma, C.; Zaino Iii, L. P.; Bohn, P. W. Self-induced redox cycling coupled luminescence on nanopore recessed disk-multiscale bipolar electrodes. *Chem. Sci.* **2015**, *6*, 3173−3179.
(24) Kang, S.; Nieuwenhuis, A. F.; Mathwig, K.; Mampallil, D.; Lemay, S. G. Electrochemical Single-Molecule Detection in Aqueous Solution Using Self-Aligned Nanogap Transducers. *ACS Nano* **2013**, *7*, 10931−10937.
(25) Zevenbergen, M. A. G.; Singh, P. S.; Goluch, E. D.; Wolfrum, B. L.; Lemay, S. G. Stochastic Sensing of Single Molecules in a Nanofluidic Electrochemical Device. *Nano Lett.* **2011**, *11*, 2881−2886.
(26) Sun, P.; Mirkin, M. V. Electrochemistry of individual molecules in zeptoliter volumes. *J. Am. Chem. Soc.* **2008**, *130*, 8241−8250.
(27) Fan, F.-R. F.; Bard, A. J. Electrochemical Detection of Single molecules. *Science* **1995**, *267*, 871−874.
(28) Kastner, M. A. The single-electron transistor. *Rev. Mod. Phys.* **1992**, *64*, 849−858.
(29) Grabert, H.; Devoret, M. H. *Single Charge Tunneling: Coulomb Blockade Phenomena in Nanostructures*; Springer US, 2013.
(30) Pajkossy, T.; Kolb, D. M. Double layer capacitance of Pt(111) single crystal electrodes. *Electrochim. Acta* **2001**, *46*, 3063−3071.
(31) Kaiser, K. L. *Electromagnetic Compatibility Handbook*; CRC Press, 2004; p 2568.
(32) Gustavsson, S.; Leturcq, R.; Simovič, B.; Schleser, R.; Ihn, T.; Studerus, P.; Ensslin, K.; Driscoll, D. C.; Gossard, A. C. Counting Statistics of Single Electron Transport in a Quantum Dot. *Phys. Rev. Lett.* **2006**, *96*, 076605.
(33) Levitov, L. S.; Lee, H.; Lesovik, G. B. Electron counting statistics and coherent states of electric current. *J. Math. Phys.* **1996**, *37*, 4845−4866.
(34) Newman, J. Resistance for Flow of Current to a Disk. *J. Electrochem. Soc.* **1966**, *113*, 501−502.
(35) Jones, G.; Bradshaw, B. C. The Measurement of the Conductance of Electrolytes. V. A Redetermination of the Conductance of Standard Potassium Chloride Solutions in Absolute Units. *J. Am. Chem. Soc.* **1933**, *55*, 1780−1800.
(36) O'Brien, G. A.; Quinn, A. J.; Biancardo, M.; Preece, J. A.; Bignozzi, C. A.; Redmond, G. Making Electrical Nanocontacts to Nanocrystal Assemblies: Mapping of Room-Temperature Coulomb-Blockade Thresholds in Arrays of 28-kDa Gold Nanocrystals. *Small* **2006**, *2*, 261−266.
(37) Pashkin, Y. A.; Nakamura, Y.; Tsai, J. S. Room-temperature Al single-electron transistor made by electron-beam lithography. *Appl. Phys. Lett.* **2000**, *76*, 2256−2258.
(38) Zheng, H.; Asbahi, M.; Mukherjee, S.; Mathai, C. J.; Gangopadhyay, K.; Yang, J. K. W.; Gangopadhyay, S. Room temperature Coulomb blockade effects in Au nanocluster/pentacene single electron transistors. *Nanotechnology* **2015**, *26*, 355204.
(39) Manheller, M.; Karthäuser, S.; Waser, R.; Blech, K.; Simon, U. Electrical Transport through Single Nanoparticles and Nanoparticle Arrays. *J. Phys. Chem. C* **2012**, *116*, 20657−20665.
(40) Greshnykh, D.; Frömsdorf, A.; Weller, H.; Klinke, C. On the Electric Conductivity of Highly Ordered Monolayers of Monodisperse Metal Nanoparticles. *Nano Lett.* **2009**, *9*, 473−478.
(41) Laaksonen, T.; Ruiz, V.; Liljeroth, P.; Quinn, B. M. Quantised charging of monolayer-protected nanoparticles. *Chem. Soc. Rev.* **2008**, *37*, 1836−1846.
(42) Quinn, B. M.; Liljeroth, P.; Ruiz, V.; Laaksonen, T.; Kontturi, K. Electrochemical resolution of 15 oxidation states for monolayer protected gold nanoparticles. *J. Am. Chem. Soc.* **2003**, *125*, 6644−6645.

DOI: 10.1021/acs.jpcc.6b04767
J. Phys. Chem. C 2016, 120, 22777−22783